Front. Earth Sci. 2025, 19(2): 275–290
https://doi.org/10.1007/s11707-024-1138-6

RESEARCH ARTICLE

Formation process of extremely thick coal seams in terrestrial basin: a case study from Saishiteng Coalfield, northern Qaidam Basin, China

Haihai HOU (✉)[1,2], Xiangqin HUANG[1], Guodong LIANG[1], Qian HE[1]

1 College of Mining, Liaoning Technical University, Fuxin 123000, China
2 Liaoning Key Laboratory of Green Development of Mineral Resources, Fuxin 123000, China

© Higher Education Press 2024

Abstract Sequence stratigraphy and coal petrology can be used to comprehensively analyze the mechanism of extremely thick coal seams under the influence of the paleo-climate, paleo-environment, and accommodation space during a coal-forming period. Based on the vertical variations in coal quality, macerals, and lithology, key sequence surfaces were identified, including the terrestrialization surface (TeS), paludification surface (PaS), give-up transgressive surface (GUTS), accommodation reversal surface (ARS), exposure surface (ExS), and flooding surface (FS) in thick coal seams of the Middle Jurassic Dameigou Formation in the Saishiteng Coalfield, northern Qaidam Basin. Using these key sequence surfaces, thick terrestrial coal seams can be divided into several wetting-up and drying-up cycles. In general, the vitrinite content, vitrinite/inertinite ratio (V/I), and gelification index (GI) increased from bottom to top, whereas the inertinite content decreased in the wetting-up cycles. The vertical stacking pattern considers the PaS as the bottom boundary, and the GUTS or ARS as the top boundary, representing an increasing trend in the accommodation space. However, the vitrinite content, V/I, and GI values decreased from the bottom to the top, whereas the inertinite content increased during the drying-up cycle. Another vertical stacking pattern started from the TeS, with the ExS or ARS as the top boundary, representing a decreasing trend in the accommodation space. The thick coal seams at the edge of the Saishiteng Coalfield are blocked by a large number of clastic sediments, whereas relatively few clastic sediments are found in the coalfield center; thus, a single extremely thick coal seam with good continuity can be formed. Based on the coal petrology and sequence stratigraphic analyses, a model of extremely thick coal seams superimposed on multiple peatlands was established from the basin margin to the basin center. Four to five drying-up and wetting-up cycles were predicted in accumulation variation. During a water transgression stage, new peat accumulates on the land, corresponding to a wetting-up cycle. In a water regression stage, new peat accumulates in the basin center, corresponding to a drying-up cycle. Analysis of the genesis of thick coal seams is important for the in-depth excavation of geological information during the coal-forming period and for coal resource exploration in terrestrial basins.

Keywords Northern Qaidam Basin, coal seams, coal petrology, sequence stratigraphy, accommodation space

1 Introduction

Coal is a common solid energy source, but a highly sensitive sediment. Geological information in coal records paleo-environmental evolution and paleo-climatic fluctuations at high resolution during coal-forming periods (Oskay et al., 2016; Dai et al., 2020; Zhang et al., 2020; Hou et al., 2022). In particular, the geological information contained in thick seams is more abundant, because the evolution from peat to coal seams occurs from continuous compaction (Ryer and Langer, 1980; Lu et al., 2018). Studying the genetic mechanism of thick coal seams cannot only reveal the paleo-environment and paleo-climate of the coal-forming period with the help of geological information contained in coals (Greb, 2013; Falahatkhah et al., 2021; Shao et al., 2021; Wang et al., 2022), but also guide the exploration and mining of coal resources in a basin.

An extremely thick coal seam has a thickness of more than 8 m. For the coal-forming model and the distribution of thick coal seams under different sequence stratigraphic

Received May 7, 2024; accepted November 20, 2024

E-mail: houmensihai@163.com

frameworks, scholars have proposed that the lowstand system tract is the main coal-forming site in parts of the region. For most basins, transgressive and highstand system tracts are conducive to the formation of thick coal seams (Diessel, 2010; Lv et al., 2023). Owing to changes in the sedimentary environment, the distribution characteristics and accumulation mechanisms of coal seams are different. Based on sequence stratigraphic analysis, episodic coal accumulation, transgressive processes, transgressive events, and lag time models of marine limestone beds have been proposed by different researchers (Shao et al., 2003, 2021; Yang et al., 2006). The concept of an "accommodation space" refers to a theoretical basis for further understanding the mechanism of coal accumulation (Jervey, 1988; Shao et al., 2021). A previous study found that coal thickness depends on the relative equilibrium between the increasing accommodation and peat accumulation rates. However, an extremely rapid or slow rise rate at the base level is not conducive to the formation of a thick coal seam (Bohacs and Suter, 1997). On this basis, different types of discontinuities in extremely thick coal seams have been identified and the discontinuity surfaces divided into exposure and flooding surfaces (ExS and FS), emphasizing that the formation of extremely thick coal seams underwent multiple sedimentary discontinuities (Jerrett et al., 2011a).

The formation of thick coal seams has attracted the attention of coal geologists worldwide. Shearer et al. (1994) suggested that most of the thick coal seams were superimposed by ancient peat bodies. The genetic mechanism of thick coal seams has been studied in transitional environments, and it has been found that macerals change regularly with increasing or decreasing accommodation space, allowing various types of sedimentary discontinuities to be identified (Li et al., 2020). The accommodation space above the terrestrialization surface (TeS) gradually decreases, representing the beginning of a drying-up cycle, which can be identified as a non-hiatal surface. The ExS is hiatal and is formed by peat exposure and oxidation, representing the end of the drying-up cycle (Wang et al., 2020). The accommodation space above the paludification surface (PaS) gradually increases, representing the beginning of a wetting-up cycle, which may be hiatal or non-hiatal surfaces. The give-up transgressive surface (GUTS) is non-hiatal and is caused by a slow increase in accommodation space. In contrast, the FS is hiatal and is caused by a sudden increase in accommodation space, representing the end of the wetting-up cycle (Davies et al., 2005; Zainal Abidin et al., 2022a) (Fig. 1). A previous investigation found that thick peats move quickly to humification and gelification under continuous dry-wet cycles by analyzing maceral petrology and coal sequence stratigraphic characteristics. Paleoenvironmental changes give rise to the accumulation and transformation of organic matter, resulting in the formation of thick peat deposits (Mangi et al., 2023). In addition, the allochthonous accumulation coal formation model cannot be ignored. When studying the genetic mechanism of thick coal seams in fault basins, several

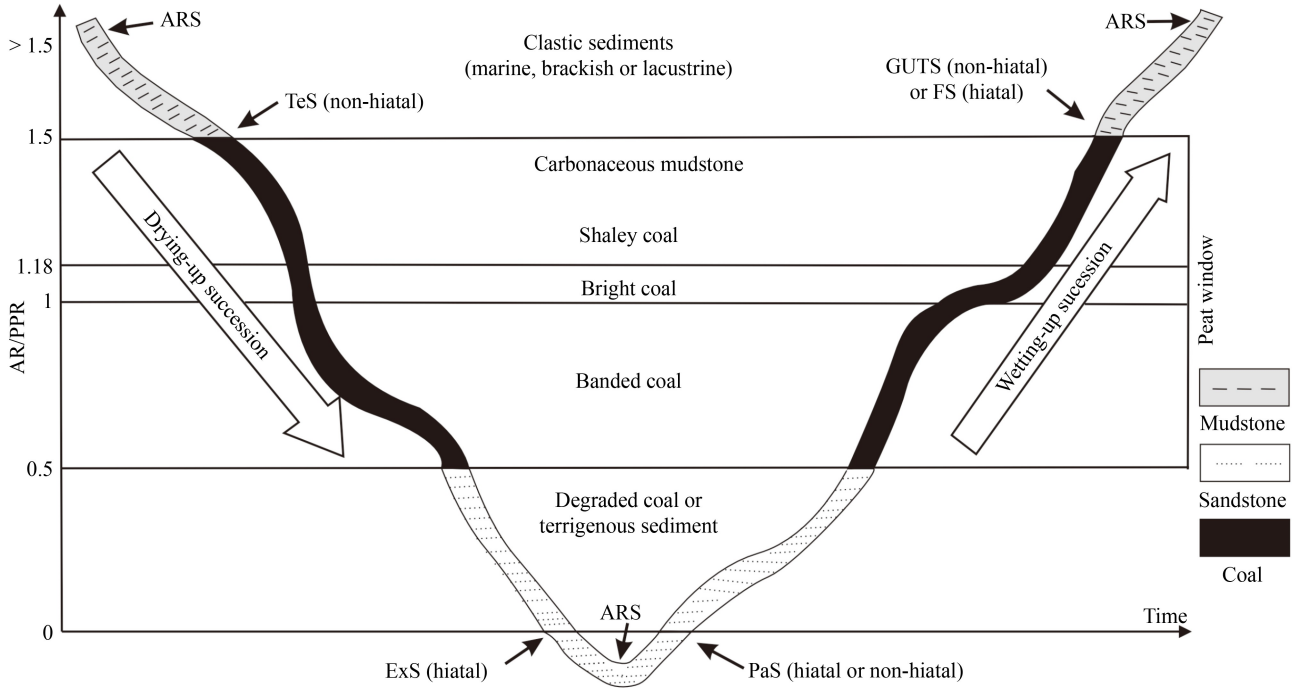

Fig. 1 Relationship between accommodation space change and peat accumulation rates (modified from Jerrett et al., 2011b). ARS: Accommodation reversal surface; TeS: Terrestrialization surface; PaS: Paludification surface; GUTS: Give-up transgressive surface; FS: Flooding surface; ExS: Exposure surface; and AR/PPR: Accommodation rate/Peat production rate.

scholars have found gravity flows and underwater debris flows in thick coal seams, indicating that peat accumulation was affected by storms, slumps, and other events, and then transported and accumulated again (Wang and Wang, 2000; Wu et al., 2007). Peat accumulation is closely related to the paleoclimate, and scholars have proposed a coal accumulation model controlled by paleoclimate evolution (Hou et al., 2023a, 2023b) and astronomical-forcing superimposed multi-staged swamp models (Wang et al., 2020). Additionally, the coal accumulation model and its processes are influenced by diverse factors; thus, a multiple coal-forming theoretical model has been proposed (Li et al., 2015).

To analyze the formation process of extremely thick coal seams in a terrestrial basin, this study considered the Beiloutian exploration area of the Saishiteng Coalfield in the northern Qaidam Basin. Based on proximate analysis, macro-lithotypes, and maceral identification, changes in coal facies and coal quality parameters under different sequences were analyzed. The super-thick coal seam model in the terrestrial basin was established from the basin margin to the center, which is important for guiding the exploration of coal resources in terrestrial basins and analyzing the genesis of super-thick coal seams in continental basins with similar geological conditions in other regions.

2 Geological setting

The Qaidam Basin, located on the north-eastern Qinghai-Xizang Plateau, belongs to the southern Tarim-China-Korea Plate and is the third largest inland basin in China. Since the Proterozoic, the Qaidam Basin has undergone multi-stage tectonic transformations, including the Caledonian, Hercynian, Indosinian, Yanshan, and Himalayan (Li et al., 2022). The Qaidam Basin is separated from the surrounding tectonic units by large faults, which are bounded by the Zongwulongshan-Qinghai Nanshan Fault in the north, the Tarim Basin and Altun Mountains in the west, the Qinling Orogenic Belt and Elashan Fault to the east, and the Kunbei Fault and East Kunlun Orogenic Belt in the south (Hu et al., 2022). The northern Qaidam Basin is rich in coal, oil, and gas resources (Hou et al., 2021) and can be divided from west to east into the Saishiteng (Saishiteng Depression), Yuqia (western Yuqia-Hongshan Depression), Dameigou (eastern Yuqia-Hongshan Depression), and Delingha Coalfields (Delingha Depression) (Fig. 2(a)). The Beiloutian exploration area is located in the Saishiteng Coalfield (Fig. 2(b)), with a strike of 13°NW and dip of 58°−61° (Li et al., 2016).

The Laogaoquan coal mine is located in the center of the Beiloutian exploration area, Saishiteng Coalfield, northern Qaidam Basin. The Jurassic substratum in the Laogaoquan coal mine is primarily composed of Devonian gray-white and gray-brown tuff. The Middle Jurassic can be divided into three third-order sequences, which correspond to the Dameigou Formation, the lower part of the Shimengou Formation, and the upper part of the Shimengou Formation. The Dameigou Formation was the object stratum in this study. The lower part was deposited in the meandering channel from the upper delta plain to the sediments of gray-white coarse sandstone. The developed thick and recoverable M7 coal seam was found in the middle section of the Dameigou Formation with a thickness of 23.33−43.57 m (average 30.73 m). The upper section was deposited in the estuary bar of the delta front, and the inter-distributary bay and channel were deposited in the lower delta plain. The sediments of the Dameigou Formation are primarily gray-white coarse sandstone, fine sandstone, siltstone, and the M7 and M6 coal seams. The lower part of the Middle Jurassic Shimengou Formation was deposited in the meandering channel and marsh of the upper delta, with sediments mainly consisting of gray coarse sandstone, fine sandstone, and the M5 coal seam. The sediments in the upper part of the Shimengou Formation are mainly siltstone, mudstone, and the M4 coal seam (Liu et al., 2013; Fig. 3).

3 Sampling and methods

Thirty-six samples were collected from the M7 coal seam in the Laogaoquan coal mine and numbered G1−G36 from west to east (from top to bottom) with a sampling interval of approximately 0.5 m (Fig. 2(c)). To prevent the contamination and oxidation of fresh samples, all samples were immediately stored in sealed bags after collection. All samples were crushed and sieved, and the coal bricks were used in the laboratory. All experiments were performed at the Geological Experiment Center of Liaoning Technical University.

3.1 Macroscopic type

The spatial distributions of the macroscopic lithotype components can be determined based on the physical properties of coal, including color, streak, luster, hardness, and fractures. Specifically, they were divided into seven macroscopic lithotypes: bright (B), bright and semi-bright (B and S-B), semi-bright (S-B), semi-bright and semi-dull (S-B and S-D), semi-dull (S-D), semi-dull and dull (S-D and D), and dull (D). The proportions of vitrain and bright coal were >80%, 65%−80%, 50%−65%, 35%−50%, 20%−35%, 10%−20%, and <10%, respectively.

3.2 Maceral identification

The coal samples were observed under an OLYMPUS BX51 polarizing microscope (objective lens 50×,

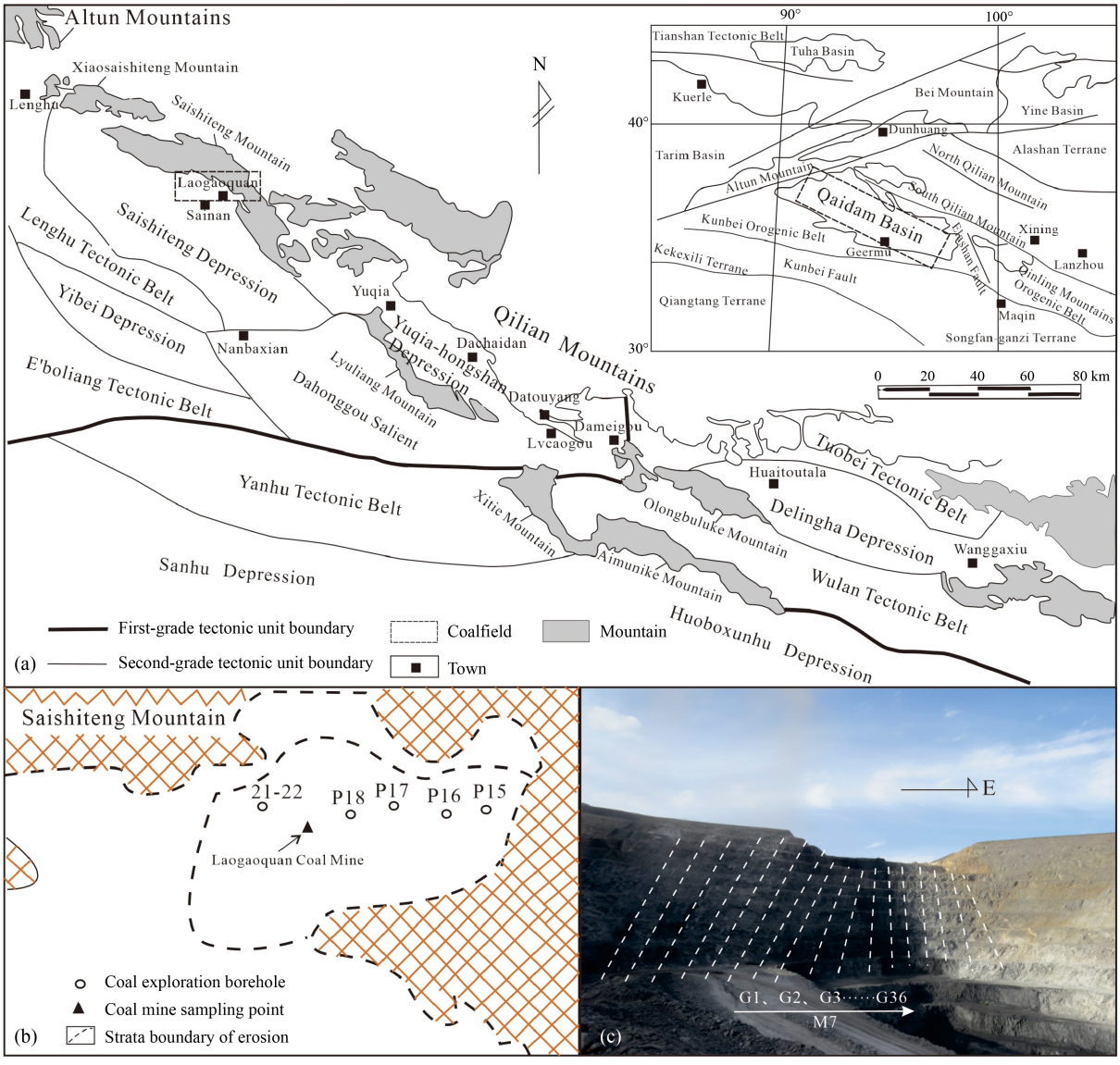

Fig. 2 Structural division and sampling locations in the northern Qaidam Basin. (a) Structural location and unit division of the northern Qaidam Basin. (b) Borehole location in the Beiloutian exploration area of the Saishiteng Coalfield. (c) Sampling location in Laogaoquan coal mine.

eyepiece 10×) under reflected light. Color and structure are commonly used to identify coal macerals. The vitrinite is shown in gray to light gray, in which the outline of the telocollinite is clear, and the composition is uniform. The inertinite is bright white in color, in which the cell structure of the fusinite is well preserved, but the semifusinite is poorly preserved. The point and row spacings were 0.5 mm with more than 500 effective measuring points. To reduce errors, three measurements were required for each sample, and the average value was used.

3.3 Proximate analysis

The ash yield, moisture content, and volatile and fixed carbon contents of the coal samples were obtained using proximate analysis. The moisture content was calculated by the mass loss that occurred coal samples were heated to 105°C–110°C under an N_2 atmosphere. The ash yield was determined by the mass of the residue measured after the coal samples were heated to 815 ± 10°C under an N_2 atmosphere. Then, 1 g of dried coal sample with particle size less than 0.2 mm was heated for 7 min at 900 ± 10°C in isolated air. The volatile fixed carbon content was calculated using the mass conservation principle.

4 Results

4.1 Coal petrology

4.1.1 Macroscopic lithotype

The macroscopic lithotypes of the M7 coal seam are

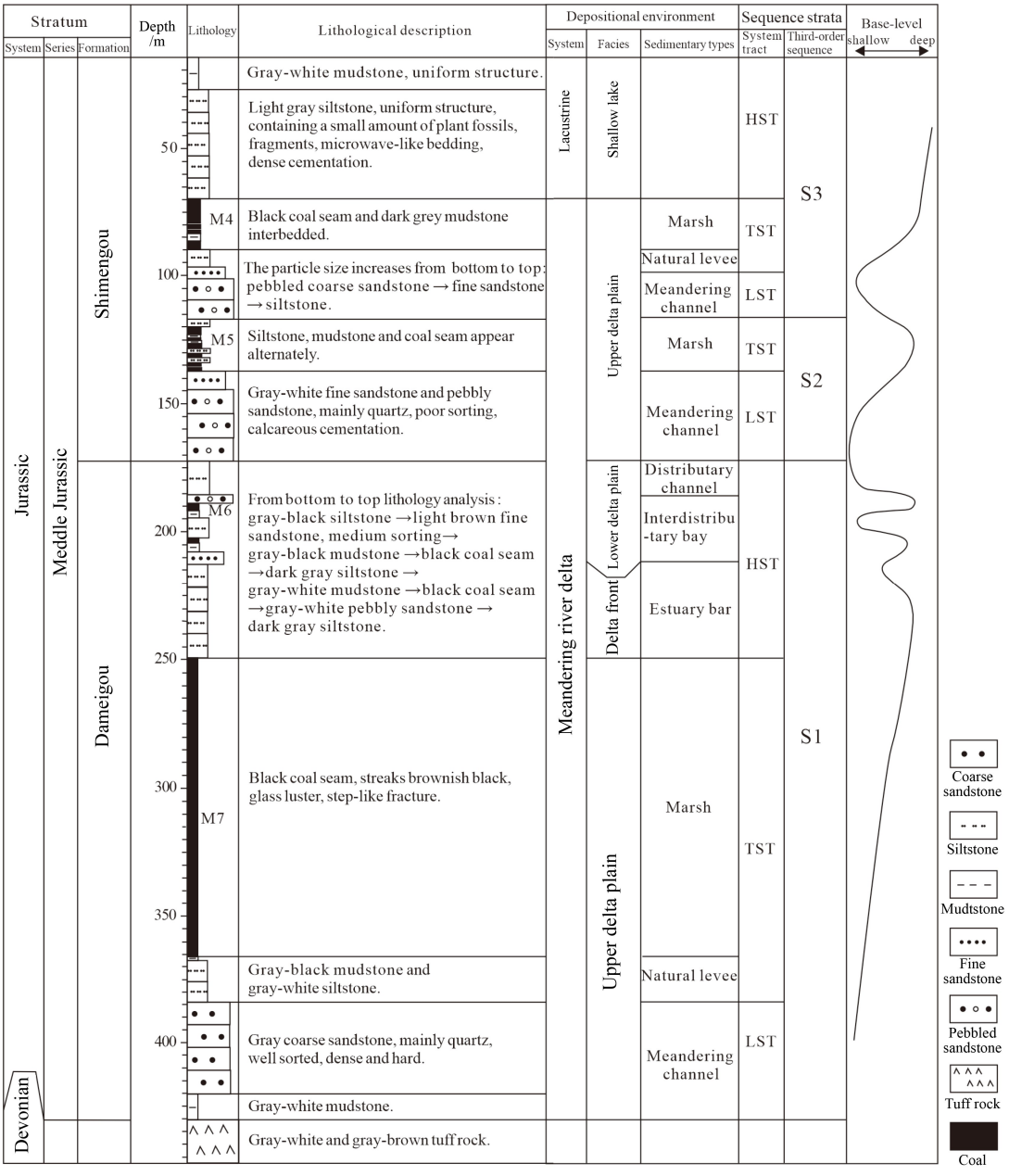

Fig. 3 Lithofacies, depositional facies, and sequence stratigraphy of the Middle Jurassic strata in Laogaoquan Coal Mine, northern Qaidam Basin (modified after reference Liu et al., 2013). HST: Highstand systems tract; TST: Transgressive systems tract; and LST: Lowstand systems tract.

mainly S-B and S-D, with the number of eleven type S-B and S-D, eight type S-B, and eight type S-D (Table 1). Vertically, the macrolithotypes of the coal samples from G36 to G33 changed from S-D to B and S-B; G26 to G22 changed from D to B and S-B; G19 to G11 changed from D to B; G8 to G4 changed from S-D to S-B; and G2 to G1 changed from S-D and D to B and S-B. Therefore, the coal gloss gradually became brighter, corresponding to the wetting-up cycle. The macrolithotypes of the coal samples from G33 to G26 and G22 to G19 changed from B and S-B to D, G11 to G8 changed from B to S-D, and G4 to G2 changed from S-B to S-D and D. Therefore, the gloss gradually became dull, corresponding to the drying-up cycle.

4.1.2 Macerals analysis

The maceral composition of the M7 coal seam is dominated by vitrinite (average 77.71%). The submaceral of vitrinite primarily contains desmocollinite and telocollinite at 13.62%−68.86% (average 37.56%) and 5.59%−71.70% (average 26.99%), respectively. The telinite and vitrodetrinite were less abundant, with percentages of 0−40.78% (average 7.38%) and 0−15.22%

Table 1 Macrolithotypes, proximate analysis, and coal maceral parameters of the Laogaoquan coal samples, northern Qaidam Basin.

Sample	Macrolithotypes	Proximate analysis/%						Vitrinite/%							Inertinite/%						V/I
		M_{ad}	A_{ad}	V_{ad}	FC_{ad}	A_d	V_d	T	C1	C2	C3	C4	VD	Total	SF	F	Mi	Ma	ID	Total	
G1	B and S-B	3.19	1.62	34.66	60.53	1.67	35.80	2.93	49.45	36.08	0.00	0.00	0.55	89.01	5.86	2.75	0.00	0.37	0.73	9.71	9.17
G2	S-D and D	3.09	4.22	28.66	64.03	4.35	29.57	1.21	28.34	33.20	0.00	0.00	0.81	63.56	15.59	0.81	0.00	0.00	18.83	35.22	1.80
G3	S-B and S-D	2.97	1.40	34.83	60.88	1.44	35.90	2.30	47.79	30.71	0.19	0.00	0.38	81.38	4.61	1.92	5.57	0.38	2.88	15.36	5.30
G4	S-B	3.07	1.32	29.43	66.10	1.36	30.36	15.26	44.33	24.95	0.41	0.00	0.41	85.36	4.74	0.00	0.00	0.00	9.07	13.81	6.18
G5	S-D	3.05	3.86	25.33	67.76	3.98	26.13	8.69	21.81	34.75	0.74	0.18	6.47	72.64	12.75	0.55	0.92	1.48	10.54	26.25	2.77
G6	S-B and S-D	2.52	3.96	34.48	59.04	4.06	35.37	1.53	31.61	33.72	0.00	0.00	0.00	66.86	15.13	8.05	4.02	0.38	2.49	30.08	2.22
G7	S-B and S-D	2.21	21.11	24.82	51.86	21.59	25.38	0.74	58.82	22.06	0.00	0.00	8.82	90.44	2.94	0.00	2.21	2.21	2.21	9.56	9.46
G8	S-D	2.69	4.46	30.68	62.17	4.58	31.53	8.54	16.75	18.09	5.70	0.00	12.56	61.64	8.04	9.38	2.18	2.35	6.87	28.81	2.14
G9	S-B	2.56	3.08	36.57	57.79	3.16	37.53	0.00	39.81	21.54	0.19	0.00	1.73	85.00	10.00	0.00	0.00	0.00	5.00	15.00	5.67
G10	S-B	2.81	4.29	29.81	63.09	4.41	30.67	20.33	21.26	25.88	0.00	0.00	2.22	69.69	16.82	1.29	0.00	1.66	9.61	29.39	2.37
G11	B	2.93	3.93	35.26	57.88	4.05	36.32	23.91	44.97	17.65	0.00	0.00	1.90	88.43	4.93	0.00	0.00	0.00	3.23	8.16	10.83
G12	S-B	3.15	6.15	23.34	67.36	6.35	24.10	2.50	11.37	55.30	0.77	0.00	15.22	85.16	3.47	2.89	0.19	0.58	1.73	8.86	9.61
G13	S-B	3.06	2.65	34.87	59.42	2.73	36.97	2.50	42.77	33.53	0.00	0.00	0.19	79.00	10.98	4.82	1.93	0.00	0.96	18.69	4.23
G14	S-D	3.41	5.22	22.07	69.30	5.40	22.85	2.60	21.56	54.65	7.62	0.00	0.00	86.43	3.72	1.86	0.00	0.00	6.69	12.27	7.04
G15	S-B and S-D	3.16	1.42	32.60	62.82	1.47	33.66	1.07	33.51	38.68	0.18	0.36	1.60	75.40	13.90	3.39	4.10	0.53	1.78	23.71	3.18
G16	S-D	2.64	1.97	33.67	61.72	2.02	34.58	8.27	12.03	36.84	0.94	0.00	6.20	64.29	14.29	0.00	0.00	0.75	20.30	35.34	1.82
G17	S-B and S-D	3.05	3.23	33.00	60.72	3.33	34.04	12.19	29.96	15.29	4.55	0.00	8.68	70.66	10.33	5.58	1.24	2.89	4.75	24.79	2.85
G18	S-B and S-D	3.44	3.02	24.86	68.68	3.13	25.75	9.92	28.60	28.60	5.25	0.00	12.26	84.63	7.20	0.78	0.58	0.97	4.86	14.40	5.88
G19	D	3.04	3.94	27.58	66.44	4.03	28.44	3.08	5.59	35.26	0.00	0.00	2.31	46.24	23.51	0.00	0.00	0.19	28.32	52.02	0.89
G20	S-B	3.34	2.02	27.42	67.22	2.09	28.37	17.10	14.87	49.44	0.37	0.19	0.74	82.71	8.74	2.23	1.30	1.67	2.79	16.73	4.94
G21	S-B and S-D	3.30	3.27	30.79	64.88	3.38	31.84	1.25	13.62	68.86	0.00	0.00	0.47	84.19	7.20	5.63	1.41	0.00	0.00	14.24	5.91
G22	B and S-B	3.34	1.03	21.95	71.44	1.07	22.71	40.78	21.15	15.91	0.17	0.00	12.01	90.02	0.85	0.00	0.00	0.00	7.28	8.12	11.09
G23	S-D	3.37	2.94	22.53	71.16	3.04	23.32	14.17	20.19	40.58	0.00	0.00	10.68	85.63	9.90	0.00	0.97	0.39	3.11	14.37	5.96
G24	S-D	3.09	1.72	26.61	68.58	1.77	27.46	8.47	19.40	42.37	0.38	0.00	0.75	71.37	18.46	1.88	2.26	0.56	3.95	27.12	2.63
G25	S-D and D	3.30	4.40	21.78	70.52	4.55	22.52	12.50	12.68	47.46	1.09	0.00	11.78	85.51	1.63	0.00	0.00	0.00	12.14	13.77	6.21
G26	D	3.05	8.76	25.94	62.25	9.04	26.76	1.87	21.46	34.89	0.75	0.19	3.92	63.06	26.12	2.24	3.17	1.12	3.92	36.57	1.72
G27	D	3.07	5.07	23.01	68.85	5.23	23.74	8.46	18.42	43.23	0.94	0.00	3.38	74.44	16.92	2.07	1.13	0.38	4.89	25.38	2.93
G28	S-B and S-D	3.23	2.87	25.88	68.02	2.97	26.74	0.94	16.79	53.58	0.38	0.00	5.28	76.98	6.79	0.00	0.19	0.19	14.53	21.70	3.55
G29	S-B and S-D	3.01	3.15	26.96	66.88	3.25	27.80	7.09	15.86	51.49	0.00	0.00	8.21	82.65	2.05	0.00	0.00	0.00	14.74	16.79	4.92
G30	S-B and S-D	3.22	6.10	27.59	63.09	6.30	28.51	0.55	26.37	45.42	0.18	0.00	2.75	75.27	9.71	6.41	3.85	0.00	3.66	23.63	3.18
G31	S-B	2.94	3.40	32.36	61.30	3.50	33.34	0.38	27.79	39.70	0.19	0.00	0.57	68.62	5.67	3.59	19.09	0.76	1.51	30.62	2.24
G32	S-B	2.50	5.64	27.52	64.34	5.78	28.23	1.92	13.41	53.83	0.19	0.00	3.26	72.61	17.82	0.38	0.57	0.57	8.05	27.39	2.65
G33	B and S-B	3.02	1.70	34.07	61.21	1.75	35.13	1.34	71.70	19.50	0.00	0.00	1.34	93.88	0.76	0.57	0.96	1.15	2.10	5.54	16.94
G34	S-D	2.68	2.41	29.56	65.35	2.48	30.37	3.79	27.07	48.28	0.00	0.00	1.55	80.69	10.34	0.00	0.00	0.00	7.59	17.93	4.50
G35	S-B and S-D	2.80	3.64	24.85	68.71	3.74	25.57	13.15	17.41	52.78	0.93	0.00	3.52	87.78	9.81	0.00	0.19	0.56	1.48	12.04	7.29
G36	S-D	2.51	3.20	32.17	62.12	3.28	33.00	4.33	23.35	48.40	0.00	0.00	0.56	76.65	16.20	0.94	1.51	1.13	3.58	23.35	3.28

Notes: A_{ad}: Ash yield; M_{ad}: Moisture content; V_{ad}: Volatile; FC_{ad}: Fixed carbon; ad: Air-dried basis; d: Dried basis; T: Telinite; C1: Telocollinite; C2: Desmocollinite; C3: Corpocollinite; C4: Gelocollinite; VD: Vitrodetrinite; SF: Semifusinite; F: Fusinite; Mi: Micrinite; Ma: Macrinite; ID: Inertodetrinite; V/I: Vitrinite/Inertinite; B: Bright; S-B: Semi-bright; S-D: Semi-dull; D: Dull; B and S-B: Bright and semi-bright; S-B and S-D: Semi-bright and semi-dull; S-D and D: Semi-dull and dull.

(average 4.25%). The coal macerals contain a small amount of corpocollinite and gelocollinite, with averages of 0.89% and 0.03%, respectively. The sub-macerals of inertinite (average 20.74%) are dominated by semifusinite and inertodetrinite, with percentages of 0.76%−26.12% (average 9.94%) and 0−28.32% (average 6.56%). Furthermore, the percentages of fusinite and micrinite were 0−9.38% (average 1.94%) and 0−19.09% (average

1.65%), respectively, with a small amount of macrinite (average 0.65%) (Table 1; Fig. 4).

Vertically, the vitrinite percentage and V/I values of the coal samples increased from G36 to G33, G26 to G22, G19 to G11, G8 to G4, and G2 to G1, whereas the percentage of inertinite decreased for the wetting-up cycle. The vitrinite percentage and V/I values of the coal samples decreased from G33 to G26, G22 to G19, G11 to G8, and G4 to G2, whereas the inertinite percentage increased, corresponding to the drying-up cycle.

4.1.3 Proximate analysis

Based on the results of the proximate analysis, the M7 coals are ultra-low ash and medium volatile coals. The moisture content had a narrow range from 2.21%−3.44% (average 2.99%), reaching a maximum value in the middle of the M7 coal seam. The ash yield ranged from 1.03 to 8.76% (average 3.95%), and only the G7 coal sample had an abnormally high value. Under weak hydrodynamic conditions, terrigenous debris input is lower during swamp development, resulting in a lower ash yield (Liu et al., 2023). The volatile content and fixed carbon were 21.78%−36.57% (average 28.82%) and 51.86%−71.44% (average 64.26%), respectively (Table 1).

In terms of the wetting-up cycle, the base level increased, but the hydrodynamic force, terrigenous debris input, and ash yield decreased. Conversely, for a drying-up cycle, the base level decreased, but the hydrodynamic force, terrigenous debris input, and ash yield increased (Xu et al., 2010). The ash yield decreased for coal samples G36 to G33, G26 to G22, G19 to G11, G8 to G4, and G2 to G1, corresponding to the wetting-up cycle. The ash yield increased for coal samples G33 to G26, G22 to G19, G11 to G8, and G4 to G2, corresponding to the drying-up cycle.

4.2 Coal facies (GI and TPI)

Coal facies largely reflect the original genetic type of coal in coal-forming swamp environments (Zainal Abidin et al., 2022b; Guatame et al., 2023). Diessel (1986) established coal facies indices based on the relationship between swamp type, peat accumulation conditions, and swamp sedimentary environment, namely the gelification index (GI) and tissue preservation index (TPI).

GI is the ratio of the gelification component to the fusinization component in coal (Eq. (1)), which represents the degree of water depth of the coal-forming swamp. A high GI value indicates that the peat swamp is wet, and the water depth is deep; otherwise, it is relatively dry and shallow. TPI is the ratio of primary to destroyed macerals in vitrinite and inertinite (Eq. (2)) (Guatame and Rincon, 2021; Jiu et al., 2021), indicating the degradation intensity of plant tissues and the integrity of plant cell preservation. The high TPI value in the coals indicates that the plant structure was well preserved, and the peat paleoenvironment was humid and weakly oxidizing. A low TPI value indicates that the plant structure is poorly preserved, and the peat swamp is a dry, partially oxidized, or extremely humid environment. Therefore, when the GI and TPI values increased in the coal samples, they corresponded to a wetting-up cycle, with a decreasing trend corresponding to a drying-up cycle:

$$\mathrm{GI} = \frac{\text{Vitrinite} + \text{Macrinite}}{\text{Semifusinite} + \text{Fusinite} + \text{Inertodetrinite}}, \quad (1)$$

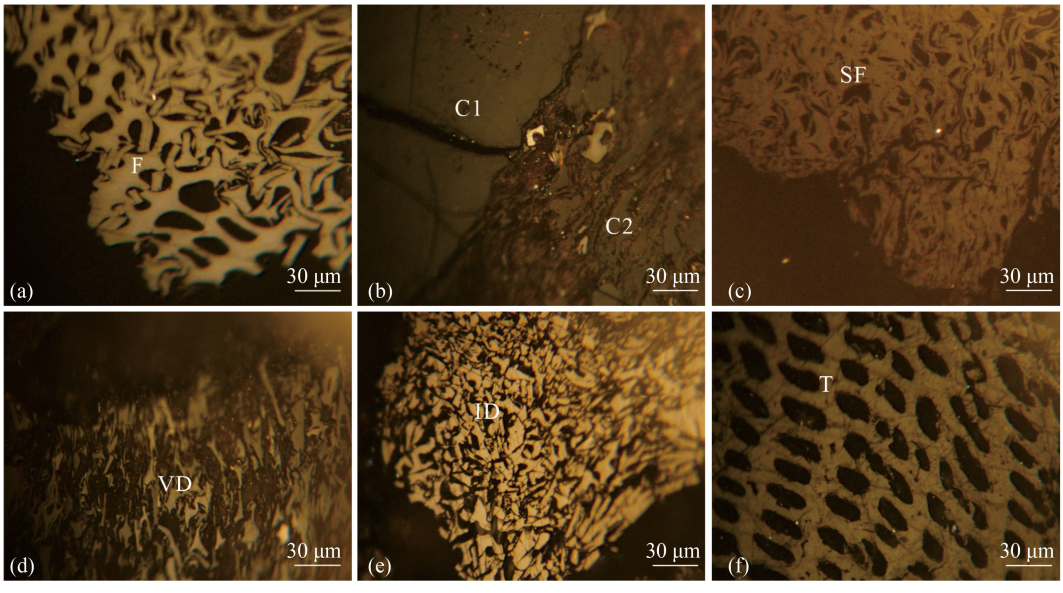

Fig. 4 Coal macerals under reflected light from the Middle Jurassic Dameigou Formation in the Laogaoquan Coal Mine, northern Qaidam Basin. T: Telinite; C1: Telocollinite; C2: Desmocollinite; VD: Vitrodetrinite; SF: Semifusinite; F: Fusinite; and ID: Inertodetrinite.

$$\mathrm{TPI}=\frac{\mathrm{Telinite}+\mathrm{Telocollinite}+\mathrm{Semifusinite}+\mathrm{Fusinite}}{\mathrm{Desmocollinite}+\mathrm{Macrinite}+\mathrm{Inertodetrinite}}. \quad (2)$$

Diessel (2007) proposed a GI-TPI diagram that has been widely used for coal facies analysis. In this study, a TPI-GI diagram was obtained by calculating the macerals of the 36 coal samples from the Laogaoquan Coal Mine (Fig. 5). The TPI values were below two for most coal samples, indicating that the microbial activity was strong during the coal-forming period, and the plant structure was poorly preserved. Most GI values exceeded one, accompanied by a peat swamp environment of moist and shallow water, indicating that the degree of gelification of the plant wood fiber tissue was stronger (Akinyemi et al., 2022). The values of GI and TPI in this study showed periodic changes, which agreed with the changes at the base level. Therefore, the peat swamp of M7 coal experienced many drying-up and wetting-up cycles.

There was a weak positive correlation between GI and TPI values. The GI value and ash yield of Sample 7 were the highest; however, the TPI of this sample is not high (Fig. 5), which could be attributed to the influence of eutrophic swamps. The GI and TPI values varied from low to high for the coal samples from G36 to G33, G26 to G22, G19 to G11, G8 to G4, and G2 to G1, owing to the change from dry to wet in the peat paleoenvironment, indicating they belonged to a wetting-up cycle. However, the GI and TPI values changed from high to low for coal samples G33-G26, G22-G19, G11-G8, and G4-G2, indicating they belonged to a drying-up cycle (Fig. 6). However, the majority of wetting-up or drying-up cycles within the GI and TIP values belong to a fluctuating change, suggesting that the paleoenvironment and paleoclimate during swamp-forming periods are not linear.

4.3 Sequence stratigraphy analysis

As the base level increased, the reduction degree of the peat swamp and gelification degree, vitrinite percentage, and coal seam gloss increased, but the inertinite percentage and ash yield decreased. In this case, semi-bright coal was the main macroscopic lithotype deposited in shallow-water forest swamp facies (Lv et al., 2023). When the base level decreases, the peat layers are susceptible to oxidation; thus, inertinite and ash yields in the coals increased (Shen et al., 2023). In this case, the macroscopic lithotypes were dominated by semi-dull or dull coal deposited in the moist forest swamp facies.

The variations in the coal facies parameters of the 36 coal samples from the Laogaoquan Coal Mine were analyzed (Table 1). From samples G36 to G33, G26 to G22, G19 to G11, G8 to G4, and G2 to G1, the vitrinite content, V/I and GI values, and base level increased, but the inertinite content and ash yield decreased, that is, they were in a wetting-up cycle. From samples G33 to G26, G22 to G19, G11 to G8, and G4 to G2, the vitrinite content, V/I and GI values, and base level decreased, but the inertinite content and ash yield increased, indicating a drying cycle. Assuming that the compaction rate from peat to coal was 6:1, the average peat sedimentation rate

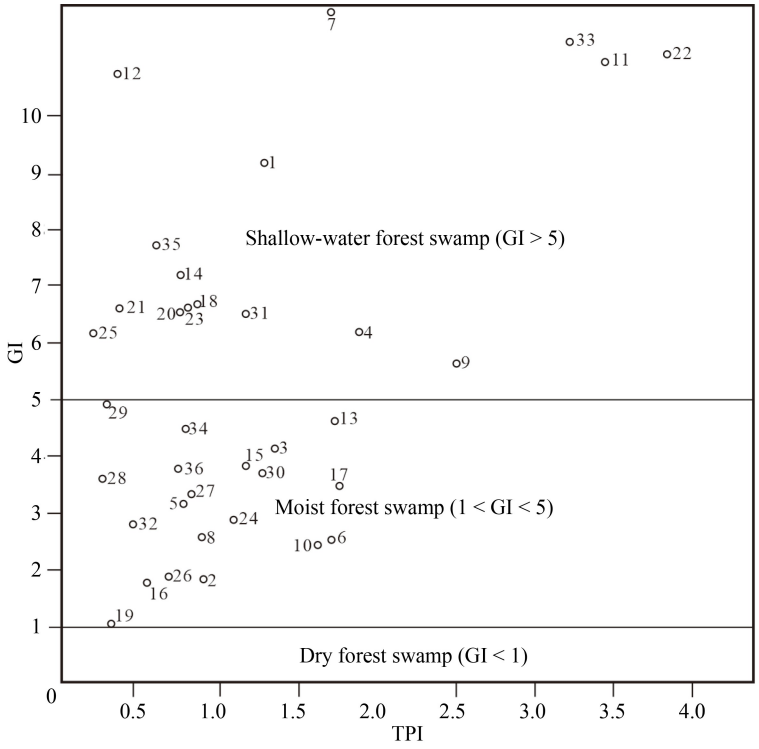

Fig. 5 TPI-GI diagram of the M7 coal seam of the Laogaoquan Coal Mine, northern Qaidam Basin.

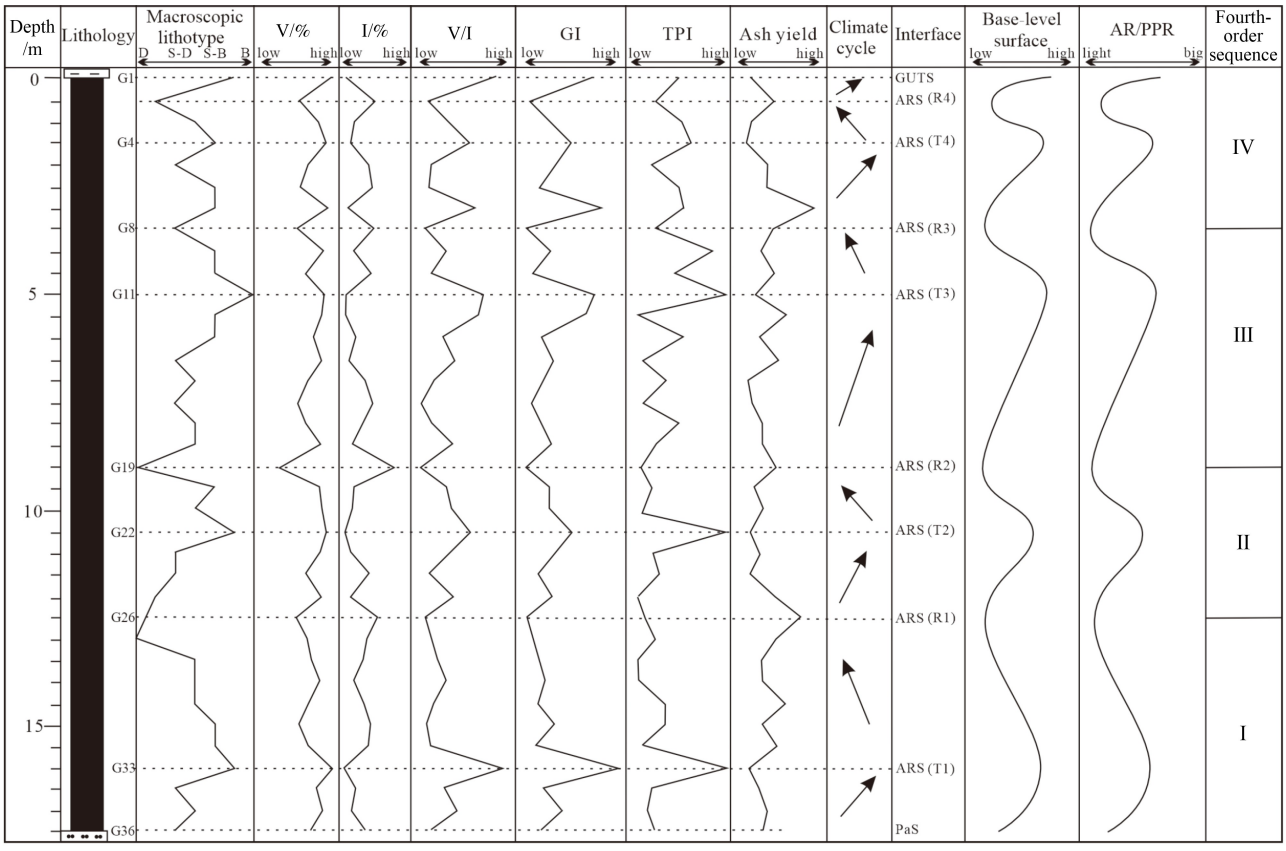

V: Vitrinite; I: Inertinite; ARS: Accommodation reversal surface; PaS: Paludification surface; ↗: Wetting-up cycle; ↖: Drying-up cycle; GUTS: Give-up transgressive surface; T1: Water-transgression discontinuity and number; R1: Water-regression discontinuity and number; AR/PPR: Accommodation Rate/Peat Production Rate; B: Bright; S-B: Semi-bright; S-D: Semi-dull; D: Dull.

Fig. 6 Coal facies evolution, base level, and AR/PPR changes in the M7 coal seam of the Laogaoquan Coal Mine, northern Qaidam Basin.

was approximately 0.2 mm/yr (Lu et al., 2018). Therefore, the duration of each drying-up and wetting-up cycle can be predicted to be 0.105−0.165 Ma, which belongs to the fourth-order sequence period (0.08−0.5 Ma). The M7 coal seam can be divided into four fourth-order sequences, with samples from G36 to G26 corresponding to Sequence I, G26 to G19 Sequence II, G19 to G8 Sequence III, and G8 to G1 Sequence IV (Fig. 6).

5 Discussion

During peat accumulation, basin subsidence rates and groundwater level variations largely determined accommodation space changes. The relationship between accommodation space and peat accumulation rate directly affects the start and termination of peat accumulation (Shen et al., 2024), which also determines its basin locations and genesis (Zhao et al., 2021). Furthermore, with an increase or decrease in groundwater level at the basin margin, the peatification process can be easily interrupted (Wang et al., 2020). For low accommodation space, peat deposited in the basin center can be continuously accumulated. There is litter parting inside the peat, which is conducive to the formation of a single thick coal seam. Based on the analysis of the lithology, accommodation space, and maceral composition from boreholes at the edge and center of the Beiloutian exploration area in the Saishiteng Coalfield, the factors controlling the formation of extremely thick coal seams in different basin positions were analyzed, and a model of extremely thick coal seams in terrestrial basins was established.

5.1 Genesis analysis of the thick coal seam

5.1.1 Basin margin

At the eastern edge of the Beiloutian exploration area in the Saishiteng Coalfield, the M7 thick coal seam developed in the lower section of the Dameigou Formation. During peat accumulation, the M7 seam in borehole P15 was vertically divided into four subseams by terrigenous clastic sediments (Fig. 7(a)). The bottom of the M7-1 seam is composed of coarse sandstones and siltstones, and the upper part is separated by siltstones. Thus, a first water-transgression and then a rapid water-

regression likely occurred (Figs. 7(a) ①–③ and 7(b) ①). The upward sediment source gradually changed to peat, corresponding to a gradual water transgression process. The M7-2 seam was formed with a rising base level and increasing accommodation space. Finally, the peat was replaced by mudstone. The process was a complete wetting-up cycle, and the top boundary was interpreted by a maximum GUTS (Figs. 7(a) ③–⑤ and 7(b) ②) (Guo et al., 2018). After a short water regression period, the base level began to rise again with peat accumulation,

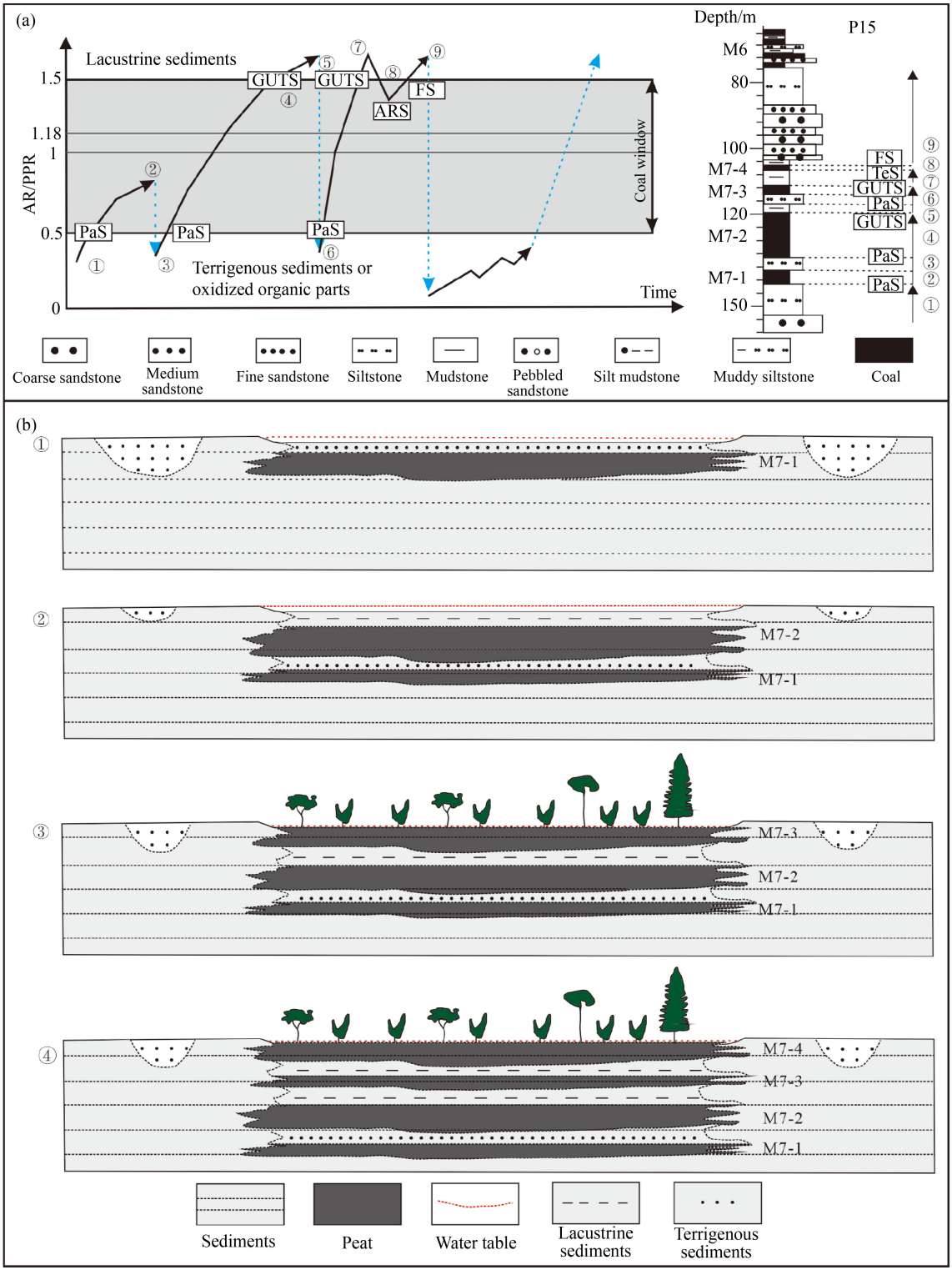

Fig. 7 Change trends in accommodation space and peatland evolution in borehole P15. (a) Change trend of accommodation space. (b) Peatland evolution.

and a PaS surface was formed. As the base level continued to rise, the peat accumulation was replaced by mudstone, forming GUTS (Figs. 7(a) ⑤–⑦ and 7(b) ③). The base level continued to rise until the ARS occurrence; then, the thinner M7-4 seam was formed after a short water-regression cycle (Figs. 7(a) ⑦–⑧ and 7(b) ④). After the deposition of the M7-4 seam, the lithology was composed of sandstones with varying grain sizes, including coarse sandstone, medium sandstone, fine sandstone and siltstone, which then transitioned upward to fine sandstone, siltstone, mudstone, and the M6 coal seam in the upper section of the Dameigou Formation (Fig. 7(a) ⑨).

Borehole P16 was closer to the basin center than borehole P15. The M7 thick coal seam was deposited in the meandering system in the lower part of the Dameigou Formation, covering the pebbled coarse sandstone of the distributary channel. During peat accumulation, owing to a gradual rise in the base level, the pebbled coarse sandstone was gradually replaced by peat. The PaS formed and was accompanied by a continuous accumulation of peat layer (Fig. 8 ①–②), indicating that the peat deposition in the basin was less affected by tectonic or terrestrial activities (Milici, 2005). Then, the coarse sandstone, fine sandstone, siltstone and M6 coal seam were formed in the upper section of the Dameigou Formation (Fig. 8 ③–⑦).

Borehole P21-22 is near the western edge of the Beiloutian exploration area. The lower section of the Dameigou Formation was primarily deposited in the delta plain, covering the interdistributary bay siltstone, fine sandstone, and mudstone (Fig. 9 ①–②). During peat accumulation, the M7 coal seam may have been affected by crevasse splay, dividing it into five layers by fine sandstone, siltstone and coarse sandstone interbed, fine sandstone, and sandy mudstone (Fig. 9) (Liu et al., 2013). The M7-1 (Fig. 9 ③), M7-2 (Fig. 9 ④), M7-3 (Fig. 9 ⑤), M7-4 (Fig. 9 ⑥), and M7-5 (Fig. 9 ⑦) coal seams were formed in a wetting-up cycle, indicating that the peat layers experienced multiple water-transgressions during peat accumulation. A peat layer is formed when the base level increases slowly, whereas terrigenous clastic sediments are formed when the base level decreases rapidly.

5.1.2 Basin center

In the east and west of the Beiloutian exploration area, the peat accumulation process was repeatedly interrupted because of the multiple effects of terrigenous debris. In the basin center, owing to the minimal influence of terrigenous debris, continuous peat layers (such as in borehole P16) can be formed under the long-term advantages of matching peat accumulation and

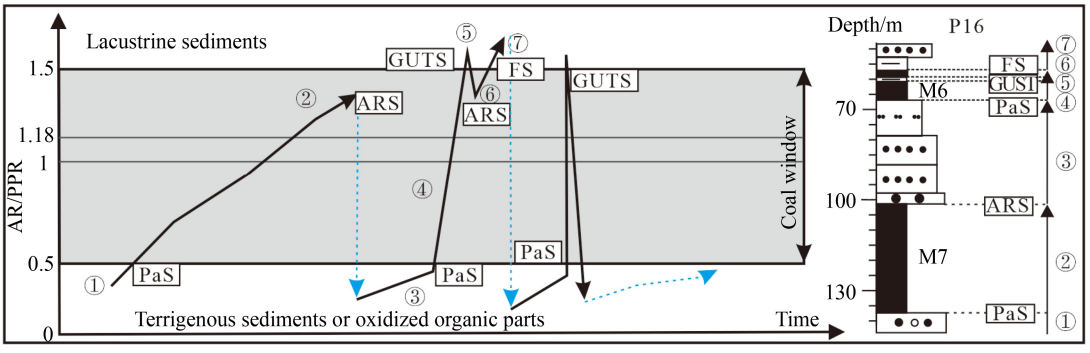

Fig. 8 Core column and change trend of the peatland accommodation space in borehole P16 (examples see Fig. 7(a)).

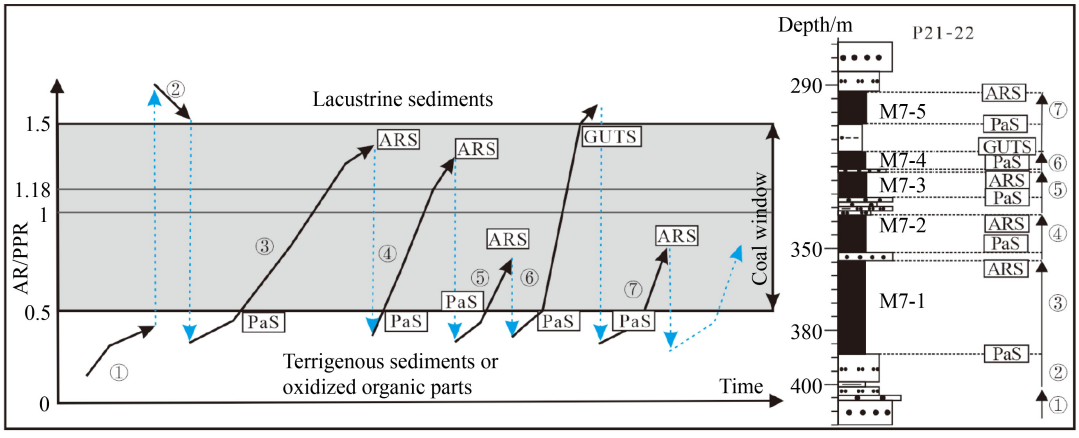

Fig. 9 Core column and change trend of peatland accommodation space in borehole P21-22 (examples see Fig. 7(a)).

accommodation rates. To further analyze the accommodation space change and dry-wet cycle transition characteristics of the peatland in a single thick coal seam, the M7 coal seam of the Laogaoquan Coal Mine in the basin center was continuously sampled. The lithology of the underlying stratum of the coal seam is siltstone, and the overlying stratum is mudstone, indicating that peat accumulation begins on the PaS and ends on the GUTS, with multiple ARS (Fig. 10).

Based on variations in the macrolithotype, maceral and coal facies parameters, and ash yield, the M7 coal seam of the Laogaoquan Coal Mine can be divided into four fourth-order sequences. Each fourth-order sequence contained a dry-wet cycle (Fig. 6). In sequence I, a wetting-up cycle occurred from coal sample G36 to G33, with increasing V/I, GI values, and coal gloss and decreasing ash yield, indicating that the ARS is close to G33 (Fig. 10(a) ①–②). However, a drying-up cycle occurred from coal samples G33 to G26, with decreasing V/I, GI values, and coal gloss and increasing ash yield, indicating that the ARS is close to G26 (Fig. 10(a) ②–③). In sequence II, the V/I and GI values, gloss, and accommodation space of coal sample from G26 to G22 increased, but the ash yield decreased under a wetting-up cycle, indicating that the ARS is near G22 (Fig. 10(a) ③–④). The V/I and GI values, gloss, and accommodation space of coal samples G22 to G19 decreased, but the ash yield decreased, representing a drying-up cycle (Fig. 10(a) ④–⑤). In sequence III, a wetting-up cycle occurred from coal sample G19 to G11, with increasing V/I, GI values, and coal gloss and decreasing ash yield, indicating that the ARS is close to G11 (Fig. 10(a) ⑤–⑥). However, a drying-up cycle occurred from coal sample G11 to G8, with decreasing

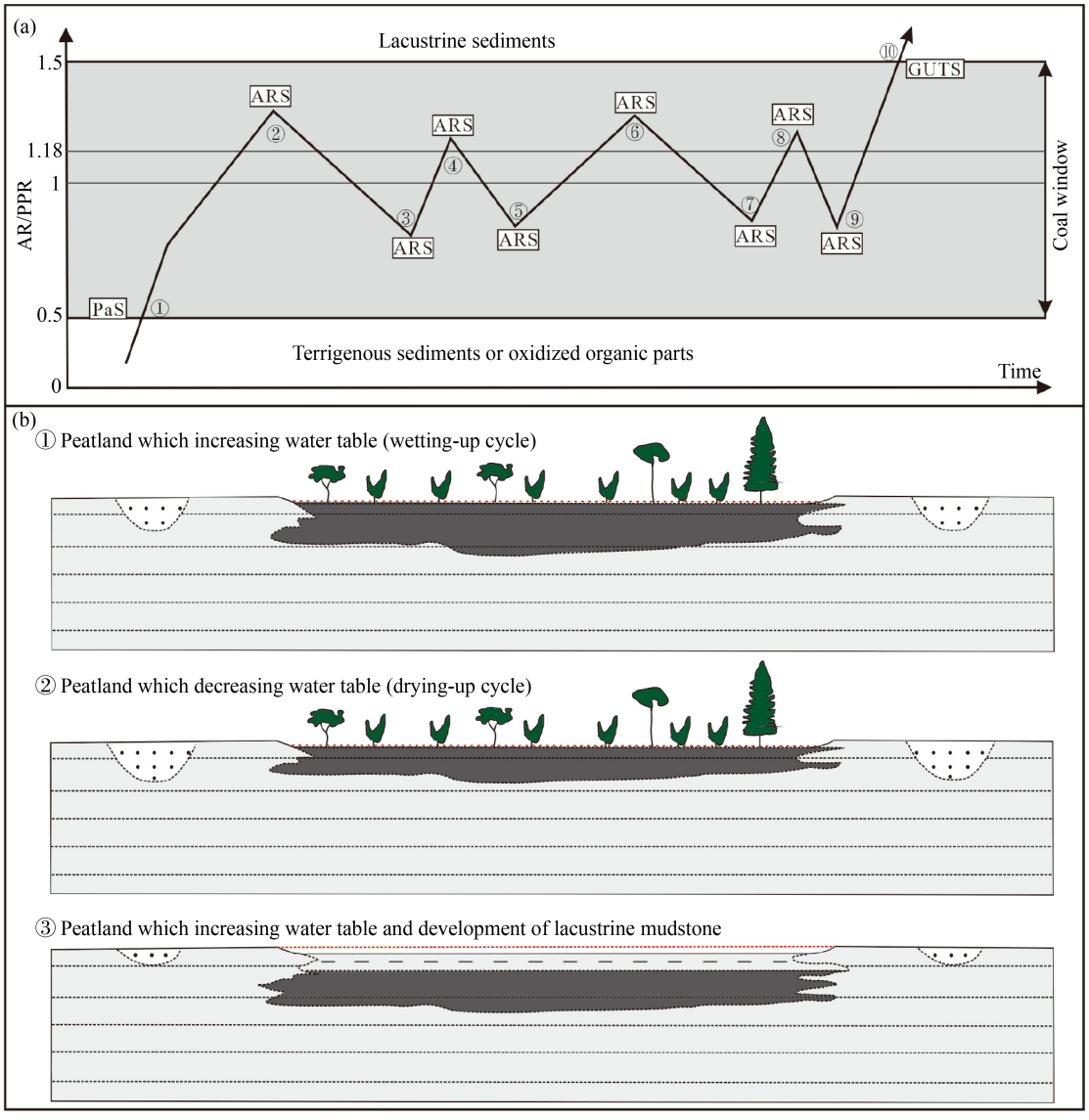

Fig. 10 Changes in peatland accommodation space and peatland evolution of the M7 coal seam in the Laogaoquan Coal Mine (see Fig. 7). (a) Change trend of peatland accommodation space. (b) Peatland evolution.

V/I, GI values, and coal gloss and increasing ash yield, indicating that the ARS is close to G8 (Fig. 10(a) ⑥–⑦). In sequence IV, the V/I and GI values, gloss, and accommodation space of coal samples from G8 to G4 increased, but ash yield decreased under a wetting-up cycle, indicating that the ARS is near G4 (Fig. 10(a) ⑦–⑧). The V/I and GI values, gloss and accommodation space of coal samples G4 to G2 decreased, with an increasing ash yield, representing a drying-up cycle (Fig. 10(a) ⑧–⑨). Coal sample G1 had higher V/I and GI values, indicating that G1 was formed in a higher accommodation space (Fig. 10(a) ⑩).

Figure 10(b) shows the deposition of the M7 coal seam in the water transgression and regression phases (Fig. 10(b) ①–②). Pealandts first began to accumulate with an increase in the base level. After several wetting-up and drying-up cycles, peatland continued to accumulate, forming a continuous thick peat layer. Finally, with the rise of base level, a sedimentary hiatus dominated by mudstone was formed (Fig. 10(b) ③).

5.2 Genetic model of thick coal seam

Based on previously proposed coal accumulation models, the vertical variation in macroscopic type, macerals, coal facies index, and ash yield of the M7 coal seam were analyzed in the northern Beiloutian exploration area of the Saishiteng Coalfield. The internal sequence interface and fourth-order sequence of the coal seam were identified, and the genetic mechanism of the extremely thick coal seam in the fourth-order sequence stratigraphic framework is comprehensively discussed. Furthermore, a model of an extremely thick coal seam was established from the basin margin to the basin center for a terrestrial basin (Fig. 11).

Borehole P15, located at the eastern basin margin, is divided into four layers by three layers of terrigenous clastic sediments. Borehole P21-22, located at the western edge of the basin, is divided into five layers by four layers of terrigenous clastic sediment. Based on observations of drilling cores and field profiles, storm and gravity flow deposition were not found in the M7 coal seam, indicating that they were mainly caused by in situ accumulation (Liu et al., 2023). When the base level rises, new peat accumulates in the land direction during a water-transgression stage, corresponding to a wetting-up cycle. The coal petrology characteristics show that the vitrinite content increases, but the inertinite content decreases, such as in samples G36 to G33, G26 to G22, G19 to G11, G8 to G4, and G2 to G1 in the M7 coal seam of the Laogaoquan Coal Mine in the center of the basin. The supply of terrigenous debris increased at the basin margin; thus, peat accumulation was replaced by parting. When the terrigenous supply weakened, there was a continuous water-transgression sedimentary transition surface. In the basin center, there was a continuous water-transgression sedimentary conversion surface, suggesting the continuous accumulation of peat (Wang et al., 2016). Therefore, extremely thick coal seams in terrestrial basins can also form via vertical superposition. Furthermore, the sedimentary environment in the basin center was likely dominated by shore-shallow lakes rather than deep and semi-deep lakes.

When the base level decreased during the regressive stage, new peat was deposited in the direction of the basin center, representing a drying-up cycle. Coal petrology is characterized by an increase in inertinite content and a decrease in vitrinite content (Shao et al., 2017), such as in samples G33 to G26, G22 to G19, G11 to G8, and G4 to G2. When the terrigenous supply was weak at the basin margin, a continuous water-regression conversion surface formed. In contrast, when the terrigenous supply was strong in the newly produced parting, a water transgression discontinuity surface formed. In the center of the basin, the M7 coal seam shows a continuous accumulation of peat, but there are also continuous

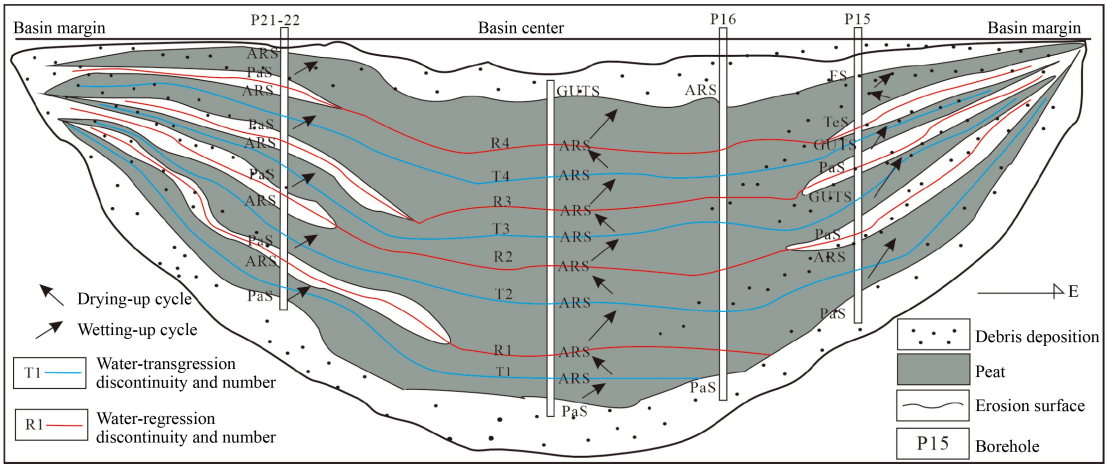

Fig. 11 Multistage peatland superimposition model of the M7 thick coal seam in the Beiloutian exploration area, Saishiteng Coalfield.

sedimentary conversion surfaces of water regression and transgression (Li et al., 2012). Based on these interfaces, nine stages of peatland development were identified, further indicating that the single thick coal seam in the terrestrial basin was composed of multiple vertically superimposed peat bodies rather than a single transgressive-regressive cycle (Fig. 11).

6 Conclusions

1) The macrolithotypes of the M7 coal seam are primarily semi-bright and semi-dull coals from the Laogaoquan Coal Mine of Middle Jurassic Dameigou Formation in the northern Qaidam Basin. Macerals were dominated by vitrinite (average 77.71%), followed by inertinite (average 20.74%). The TPI and GI values of the M7 coal seam changed periodically, indicating that the peat accumulation period occurred in a paleoenvironment of multiple water transgression and regression cycles.

2) When the base level increased, the vitrinite, V/I, GI values, and gloss increased, whereas the inertinite content decreased with mainly semi-bright coal, and the coal face belonged to the shallow-water forest swamp. When the base level decreased, the vitrinite, V/I, GI values, and gloss decreased, whereas the inertinite content increased with mainly semi-dull or dull coal, and the coal face belonged to a dry forest swamp.

3) Based on changes in coal macerals, coal quality, and coal facies, surfaces including TeS, PaS, GUTS, ARS, ExS, and FS were identified in extremely thick coal seams. The M7 thick coal seam contained a series of wetting-up and drying-up cycles bounded by discontinuities, indicating that the thick coal seam was the product of a multi-stage peat swamp with vertical superposition.

4) An extremely thick coal model under multiple peat layer overlays was established for terrestrial basins from the basin margin to the center. Owing to the influence of terrigenous debris, the basin margin was repeatedly interrupted during peat accumulation to form a parting layer. However, the basin center has relatively less terrigenous debris, with a long-term balance between peat accumulation and accommodation space, forming a single super-thick coal seam.

Acknowledgment The coal sample collection was received great assistance by Lei Liu, Xuetian Wang as well as Wenchao Shen. This study was also supported by the National Natural Science Foundation of China (Grant No. 42102223), and the basic scientific research project of Liaoning Provincial Department of Education (No. LJKMZ20220693).

Competing interests The authors declare that they have no competing interests.

References

Akinyemi S A, Adebayo O F, Madukwe H Y, Kayode A T, Aturamu A O, Olaolorun O A, Nyakuma B B, Jauro A, Gitari W M, Mudzielwana R, Hower J C (2022). Elemental geochemistry and organic facies of selected cretaceous coals from the Benue Trough basin in Nigeria: implication for paleodepositional environments. Mar Pet Geol, 137: 105490

Bohacs K, Suter J (1997). Sequence stratigraphic distribution of coaly rocks: fundamental controls and paralic examples. AAPG Bull, 81(10): 1612–1639

Dai S F, Bechtel A, Eble C F, Flores R M, French D, Graham I T, Hood M M, Hower J C, Korasidis V A, Moore T A, Puttmann W, Wei Q, Zhao L, O'Keefe J M K (2020). Recognition of peat depositional environments in coal: a review. Int J Coal Geol, 219: 103383

Davies R, Diessel C, Howell J, Flint S, Boyd R (2005). Vertical and lateral variation in the petrography of the Upper Cretaceous Sunnyside coal of eastern Utah, USA-implications for the recognition of high-resolution accommodation changes in paralic coal seams. Int J Coal Geol, 61(1−2): 13–33

Diessel C F K (1986). On the correlation between coal facies and depositional environments.In: On the correlation between coal facies and depositional environments. Proceeding 20th Symposium of Department Geology, University of New Castle, New South Wales, 19–22

Diessel C F K (2007). Utility of coal petrology for sequence-stratigraphic analysis. Int J Coal Geol, 70(1−3): 3–34

Diessel C F K (2010). The stratigraphic distribution of inertinite. Int J Coal Geol, 81(4): 251–268

Falahatkhah O, Kordi M, Fatemi V, Koochi H H (2021). Recognition of Milankovitch cycles during the Oligocene-Early Miocene in the Zagros Basin, SW Iran: implications for paleoclimate and sequence stratigraphy. Sediment Geol, 421: 105957

Greb S F (2013). Coal more than a resource: critical data for understanding a variety of earth-science concepts. Intern J Coal Geol, 118: 15–32

Guatame C, Rincon M (2021). Coal petrology analysis and implications in depositional environments from upper Cretaceous to Miocene: a study case in the Eastern Cordillera of Colombia. Int J Coal Sci Technol, 8(5): 869–896

Guatame C, Rincon M, Bermudez M A (2023). Relationship between coal composition, coal facies, and desorbed methane gas content: thermal histories and exhumation processes in the middle Magdalena Valley basin, Colombia. J S Am Earth Sci, 128: 104369

Guo B, Shao L Y, Hilton J, Wang S, Zhang L (2018). Sequence stratigraphic interpretation of peatland evolution in thick coal seams: examples from Yimin Formation (Early Cretaceous), Hailaer Basin, China. Int J Coal Geol, 196: 211–231

Hou H H, Chen H Z, Shao L Y, Pan Z Z (2023a). New understanding of coal seam distribution law: coal accumulation model controlled by paleoclimate evolution. Coal Geol Explor, 51(3): 10–18 (in Chinese)

Hou H H, Liu S J, Shao L Y, Li Y H, Zhao M E, Wang C (2021). Elemental geochemistry of the Middle Jurassic shales in the northern Qaidam Basin, northwestern China: constraints for tectonics and paleoclimate. Open Geosci, 13(1): 1448–1462

Hou H H, Shao L Y, Liang G D, Tang Y, Zhang H J, Zhang Q Q

(2022). Repeated wildfires in the Middle Jurassic Xishanyao Formation (Aalenian and Bajocian Ages) in northwestern China. Acta Geol Sin Engl Ed, 96(5): 1752–1763

Hou H H, Shao L Y, Tang Y, Li Y N, Liang G D, Xin Y L, Zhang J Q (2023b). Coal seam correlation in Terrestrial Basins by sequence stratigraphy and its implications for Paleoclimate and paleoenvironment evolution. J Earth Sci, 34(2): 556–570

Hu X Y, Wu L, Zhang Y S, Zhang J Y, Wang C W, Tang J C, Xiao A C, Chen H L, Yang S F (2022). Multiscale lithospheric buckling dominates the Cenozoic subsidence and deformation of the Qaidam Basin: a new model for the growth of the northern Tibetan Plateau. Earth Sci Rev, 234: 104201

Jerrett R M, Davies R C, Hodgson D M, Flint S S, Chiverrell R C (2011a). The significance of hiatal surfaces in coal seams. J Geol Soc London, 168(3): 629–632

Jerrett R M, Flint S S, Davies R C, Hodgson D M (2011b). Sequence stratigraphic interpretation of a Pennsylvanian (Upper Carboniferous) coal from the central Appalachian Basin, USA. Sedimentology, 58(5): 1180–1207

Jervey M T (1988). Quantitative geological modeling of siliciclastic rock sequences and their seismic expression. In: Wilgus C K et al. , eds. Sea-Level Changes- An Integrated Approach. SEPM Special Publication, 42: 14–70

Jiu B, Huang W H, Hao R L (2021). A method for judging depositional environment of coal reservoir based on coal facies parameters and rare earth element parameters. J Petrol Sci Eng, 207: 109128

Li G X, Zhu R K, Zhang Y S, Chen Y, Cui J W, Jiang Y H, Wu K Y, Sheng J, Xian C G, Liu H (2022). Geological characteristics, evaluation criteria and discovery significance of Paleogene Yingxiongling shale oil in Qaidam Basin, NW China. Pet Explor Dev, 49(1): 21–36

Li J, Zhuang X G, Zhou J B, He Y L (2012). Coal facies characteristic and identification of transgressive/regressive coal-bearing cycles in a thick coal seam of Xishanyao Formation in eastern Junggar coalfield, Xinjiang. J Jilin U (Earth Sci Ed), 42(S2): 104–114 (in Chinese)

Li M, Shao L Y, Liu L, Lu J, Spiro B, Wen H J, Li Y H (2016). Lacustrine basin evolution and coal accumulation of the Middle Jurassic in the Saishiteng coalfield, northern Qaidam Basin, China. J Palaeogeogr, 5(3): 205–220

Li Y N, Shao L Y, Fielding C R, Wang D W, Mu G Y, Luo H H (2020). Sequence stratigraphic analysis of thick coal seams in paralicenvironment-A case study from the Early Permian Shanxi Formation in the Anhe coalfield, Henan Province, north China. Int J Coal Geol, 222(1): 103451

Li Z X, Lv D W, Wang D D, Liu H Y, Wang P L, Liu Y (2015). The multiple coal-forming theoretical system and its model. Acta Geosci Sin, 36(3): 271–282 (in Chinese)

Liu T J, Shao L Y, Cao D Y, Ju Q, Guo J N, Lu J (2013). Forming-Conditions and Resource Assessment of Jurassic Coal in Northern Qaidam Basin. Beijing: Geological Publishing House, 54–79 (in Chinese)

Liu Y, Li Z X, Wang D D, Li X J, Zheng X, Liu H Y, Liu J M, Li Z Y (2023). The genetic characteristics of intermittency and continuity in peat formation and accumulation processes. Ore Geol Rev, 161: 105650

Lu J, Yang M F, Sun X Y, Shao L Y, Zhang F H (2018). Jurassic coal maceral and deposition rate of peat in the northern Qaidam Basin. J Min Sci Tech, 3(1): 1–8 (in Chinese)

Lv D W, Shen Y Y, Van Loon A J T, Raji M, Zhang Z H, Song G Z, Ren Z H, Wang Y J, Wang D D (2023). Sequence stratigraphy of the Middle Jurassic Yan'an Formation (NE Ordos Basin, China), relationship with climate conditions and basin evolution, and coal maceral's characteristics. Front Earth Sci (Lausanne), 11: 1155145

Mangi H N, Chi R A, Zhao J, Yan D T, Sindhu L, He D S, He Z X, Li J, Ashraf U, Wang H B (2023). Formation mechanism of thick coal seam in the Lower Indus Basin, SE Pakistan. Nat Resour Res, 32(1): 257–281

Milici R C (2005). Appalachian coal assessment: defining the coal systems of the Appalachian basin. Coal systems analysis. Spec Pap Geol Soc Am, 387: 9–30

Oskay R G, Christanis K, Inaner H, Salman M, Taka M (2016). Palaeoenvironmental reconstruction of the eastern part of the Karapinar-Ayranci coal deposit (Central Turkey). Int J Coal Geol, 163: 100–111

Ryer T A, Langer A W (1980). Thickness change involved in the peat-to-coal transformation for a bituminous coal of Cretaceous age in central Utah. J Sediment Res, 50(3): 987–992

Shao L Y, Wang X T, Lu J, Wang D D, Hou H H (2017). A reappraisal on development and prospect of coal sedimentology in China. Acta Sediment Sin, 35(5): 1016–1031 (in Chinese)

Shao L Y, Xu X T, Wang S, Wang D D, Gao D, Wang X T, Lu J (2021). Research progress of palaeogeography and palaeoenvironmental evolution of coal-bearing series in China. J Palaeogeogr (Chinese Ed), 23(1): 19–38 (in Chinese)

Shao L Y, Zhang P F, Gayer R A, Chen J L, Dai S F (2003). Coal in a carbonate sequence stratigraphic framework: the Upper Permian Heshan Formation in central Guangxi, southern China. J Geol Soc London, 160(2): 285–298

Shearer J C, Staub J R, Moore T A (1994). The conundrum of coal bed thickness: a theory for stacked mire sequences. J Geol, 102(5): 611–617

Shen W C, Shao L Y, Zhou Q Y, Liu J S, Eriksson K A, Kang S L, Steel R J (2024). The role of fluvial and tidal currents on coal accumulation in a mixed-energy deltaic setting: Pinghu Formation, Xihu Depression, East China Sea Shelf Basin. Sedimentology, 71(1): 173–206

Shen Y Y, Lv D W, Zhang Z H (2023). Analysis on sequence stratigraphy characteristics and main controlling factors of coal facies evolution of Yan'an Formation, Dongsheng Coalfield. Coal Geo China, 35(1): 1–6 (in Chinese)

Wang D D, Shao L Y, Liu H Y, Shao K, Yu D M, Liu B Q (2016). Research progress in formation mechanisms of super-thick coal seam. Journal of China Coal Society, 41(6): 1487–1497 (in Chinese)

Wang H, Wang G F (2000). A new accumulation model of coal seams in France Extensional Basins. J Earth Sci, 11(3): 297–301

Wang L J, Lv D W, Hower J C, Zhang Z H, Raji M, Tang J G, Liu Y, Gao J (2022). Geochemical characteristics and paleoclimate

implication of Middle Jurassic coal in the Ordos Basin, China. Ore Geol Rev, 144: 104848

Wang S, Shao L Y, Wang D D, Hilton J, Guo B, Lu J (2020). Controls on accumulation of anomalously thick coals: implications for sequence stratigraphic analysis. Sedimentology, 67(2): 991–1013

Wu C L, Li S H, Wang G F, Liu G, Kong C F (2007). The allochthonous genesis model about the extra-thick and high-quality coalbed in Xianfeng basin, Yunnan Province, China. Front Earth Sci China, 1(1): 97–105

Xu F M, Huang W H, Wu C S, Guo Y S, Wu Z J, Ao W H (2010). Coal petrology and facies of coal seam No. 39 from Dingfengshan mining district. J China Coal Soc, 35(4): 623–628 (in Chinese)

Yang R C, Han Z Z, Li Z X, Fan A P (2006). Base-level cycles and episodic coal accumulation-Case study of Dongsheng Coalfield in Ordos Basin. J China Univ Min Technol, 16(4): 439–442

Zainal Abidin N S, Mustapha K A, Abdullah W H, Hakimi M H (2022b). Coal petrology of Neogene low-rank coal in Mukah Coalfield, Sarawak, Malaysia: implications for coal facies and paleodepositional reconstructions. Arab J Geosci, 15(3): 270

Zainal Abidin N S, Mustapha K A, Abdullah W H, Konjing Z (2022a). Paleoenvironment reconstruction and peat-forming conditions of Neogene paralic coal sequences from Mukah, Sarawak, Malaysia. Sci Rep, 12(1): 8870

Zhang Z H, Wang C S, Lv D W, Hay W W, Wang T T, Cao S (2020). Precession-scale climate forcing of peatland wildfires during the early middle Jurassic greenhouse period. Global Planet Change, 184: 103051

Zhao H G, Li Y, Chang X C, Li Z X, Liu H Y, Zhao C L (2021). A comparative study of the coal-forming characteristics of marginal sea basins and epicontinental sea basins. Acta Geol Sin Engl Ed, 95(1): 121–130